

Research paper

Effect of fins and nanoparticles in the discharge performance of PCM thermal storage system with a multi pass finned tube heat exchange

João Pássaro^{a,b,*}, A. Rebola^a, L. Coelho^a, J. Conde^b, G.A. Evangelakis^c, C. Prouskas^c, D.G. Papageorgiou^c, A. Zisopoulou^c, I.E. Lagaris^c

^a Escola Superior de Tecnologia, Instituto Politécnico de Setúbal, Estefanilha, Setúbal, 2910-761, Portugal

^b Faculdade de Ciências e Tecnologia, Universidade Nova de Lisboa, Caparica, Almada, 2829-516, Portugal

^c University of Ioannina, Ioannina, 45110, Greece

ARTICLE INFO

Keywords:

CFD melting/solidification model
Finned tubes heat exchanger
Latent heat thermal storage system
Nanoparticles enhanced phase change material
Graphene nanoplatelets

ABSTRACT

This work studies the heat exchange process of a latent heat thermal energy storage (LHTES) system equipped with a compact finned tubes heat exchanger (HE) as this is one of the most important aspects of the storage system, the capacity for effectively delivering its stored energy. This work fills in a literature gap for 3D, transient heat transport fluid (HTF) flow models concerning storage systems with phase change materials (PCMs) with fins and nanoparticles allowing for an evaluation on the quality of heat delivered by the system. Numerical simulations, for full turbulent conditions of the HTF flow, were developed to access the influence of the fin pitch and the PCM thermal properties in the performance of the energy discharge process. Samples of commercial paraffin-wax A53 doped with graphene based nanoplatelets were tested and characterised. Different types of nanoplatelets were employed in the range of 0.5% to 6% weight. Measured data of the thermal conductivity, specific heat and fusion latent heat are presented. The simulations were developed for three fin pitch values 5, 10 and 20 mm and for 1%wt and 6%wt nanoparticles loads. The effect of fins and combination of fins and nanoparticles in the outlet temperature and liquid fraction distribution inside the LHTES unit during the discharge process in a 3D full scale model was analysed. The system performance was evaluated based of off the outlet temperature of HTF to ascertain both the quantity and quality of the heat provided. The results show that the PCM thermal conductivity is significantly enhanced by the addition of graphene nanoparticles with a high aspect ratio. The addition of only 1%wt doubled the solid phase PCM thermal conductivity and for a 6%wt load the thermal conductivity increased by a factor of 3.5. Meanwhile, specific and latent heat values of the samples are relatively unaffected. The numerical results further show that applying thin fins is an effective approach to enhance LHTES systems discharge performance. Increasing the fin number significantly enhances the heat transfer rate and the HTF discharge temperature during solidification and has a positive impact in the useful discharge heat capacity, providing better quality heat. Combining fins and nanoparticles improves the discharge process, nevertheless the role of nanoparticles becomes secondary as the fins number increases. The results demonstrate that standardised compact finned heat exchangers ubiquitously used in the HVAC industry can successfully overcome the low thermal conductivity of common PCMs without compromising the useful heat discharge capacity or resorting to nanoparticles decreasing the discharge time between 60 and 77% with adequate fin number.

1. Introduction

Latent heat thermal energy storage systems employing PCMs is an attractive way of storing thermal energy. Comparatively to common sensible heat storage systems, latent systems have some advantages such as a superior energy storage density in a narrow temperature range and the isothermal nature of the storage process. Despite some limitations, hydrated salts, organic paraffins and non-paraffins are the most

common PCMs for low and moderate temperature applications [1]. Hydrated salts are corrosive, have phase segregation and supercooling issues, on the other hand, organic PCMs are moderately flammable and paraffins have compatibility issues with plastic containers [1,2]. Another limitation common to both, is their poor thermal conductivity, in particular for organic PCMs, which limits LHTES systems performance and application.

* Corresponding author at: Escola Superior de Tecnologia, Instituto Politécnico de Setúbal, Estefanilha, Setúbal, 2910-761, Portugal.
E-mail address: jpap87@gmail.com (J. Pássaro).

Nomenclature

\bar{S}	Source term
A_{mushy}	Mushy zone
cp	Specific heat
H	Total enthalpy
h	Sensible enthalpy
L	Latent heat
Re_d	Reynolds number
T	Temperature
t	Time
V	Velocity
CFD	Computational Fluid Dynamics
DSC	Differential Scanning Calorimetry
GnP	Graphene Nanoplatelets
HE	Heat Exchanger
LHTES	Latent Heat Thermal Energy Storage
MDSC	Modulated Differential Scanning Calorimetry
NePCMs	Nanoparticle Enhanced Phase Changes Materials
NP	Nanoparticles
PCM	Phase Change Materials
xGnP	Exfoliated Graphite Nano-platelets
Greek	
β	Thermal expansion coefficient
γ	Liquid mass fraction
μ	Dynamic viscosity
ϕ	Volume fraction
ρ	Density
ξ	Constant
Subscripts	
0	Reference temperature
<i>inlet</i>	Inlet temperature
<i>l</i>	Liquidus phase
<i>n</i>	Nanoparticle
<i>PCM</i>	Phase Change Material
<i>s</i>	Solidus phase

To overcome this limitation different approaches have been studied, such as embed the PCMs into solid porous foams [3,4] or carbon fibre structures [5,6]. Developing nanoparticle enhanced PCMs (NePCMs), through the dispersion of high thermal conductivity metallic [7–11] or carbon-based nanoparticles [11–16] into the base PCMs is other investigated approach. The thermal conductivity enhancement can be significant with low particle load. The studies suggested that carbon-based nanoparticles seem to present advantages comparatively to metallic ones. An increase of the thermal conductivity up to 180% for 8%wt particles load was reported by Warzoha et al. [12] based on Graphite nano-fibres with a thermal conductivity of around 880 W/m K. However, the thermal conductivity enhancement was accompanied by a reduction in the fusion latent heat from 271.6 kJ/kg to 242.7 kJ/kg. Carbon nanostructures have even higher thermal conductivities and therefore are very attractive as additives to enhance PCMs thermal conductivity. A linear thermal conductivity enhancement up to 30% with negligible change in the fusion latent heat was reported by Zeng et al. [13] due to the dispersion of multi-walled nanotubes up to 5%wt into organic PCM 1-tetradecanol. The employed nanotubes had 5–15 μm length and 10–30 nm outer diameter. Li [14] studied the thermal

conductivity enhancement of a paraffin by graphite nanoparticles with 35 nm in diameter. The thermal conductivity increased from 0.13 W/m K to 0.37 W/m K and 0.96 W/m K for particles load of 1%wt and 10%wt respectively. The phase change temperature was marginally affected and the latent heat was reduced from 209.33 kJ/kg to 202.60 kJ/kg and 181.81 kJ/kg. Kim and Drzal [15] showed that exfoliated graphite nanoplatelets (xGnP-15) with diameter of 15 μm , thickness of less than 10 nm and BET surface area of around 30 m^2/g , when mixed with paraffin (n-docosane) from 1%wt up to 7%wt, increased the thermal conductivity linearly from 0.26, for the pure paraffin, to a value of 0.80 W/m K. In addition, a negligible change in the latent heat fusion and the phase change temperature was reported. This study was extended to xGnP-1 particles [16], which has a higher BET surface area, around 100–130 m^2/g . The sample's latent heat was not adversely affected by the xGnP-1 nano-platelets and the thermal stability improved. Both nano-platelets improved the thermal conductivity, but xGnP-15 presented better results. The impact of nano additives on the performance of PCMs based energy storage systems was also investigated. Khan and Khan [17] developed an experimental and numerical study in a coaxial pipe storage unit, employing different nanoparticles (Al₂O₃, AlN and GnP) and a paraffin. The three nanoparticles improved the charge and discharge rates of the storage unit, with GnP providing the best results. Additionally, it was found that increasing Al₂O₃ fraction from 1%vol to 3%vol significantly improves the system thermal performance. However, an insignificant enhancement was observed by increasing the particles load from 3%vol to 5%vol. Dhaidan et al. [18] studied the melting process of n-octadecane enhanced by CuO nanoparticles in a horizontal cylindrical capsule with heated walls. Nanoparticles load up to 5%wt were studied and different heating rates were analysed. The results showed that CuO nanoparticles enhanced the PCM effective thermal conductivity and accelerated the melting process. The benefit was more notorious at low particle loads and high heating rates. According to the Authors, the increment of the NePCM viscosity and nanoparticles agglomeration and sedimentation issues attenuated the benefits of nano additives at higher loads. In a horizontal concentric annular unit, numerical simulations showed a reduction of 9% and 16% in the full solidification time of a PCM from adding 2%vol and 4%vol of Cu nanoparticles [19].

Applying fins and combining fins with nanoparticles is another technique that has been studied to improve LHTES units' performance. Ye et al. numerically confirmed that number of fins and wall boundary conditions play an important role in the thermal performances of LHTES [20]. Deng and Ye [21] demonstrated that the melting time can be decreased between 53 and 66% employing local enhanced finned tubes. Rathod and Banerjee [22] reported a reduction in the full solidification time of a PCM up to 43.6% by attaching three longitudinal fins in the HTF circulation tube of an annulus laboratorial LHTES unit. Simulations presented by Darzi et al. [19] showed a reduction of 28%, 62%, 75% and 85% in the solidification time of a PCM by applying 4, 10, 15 and 20 longitudinal fins to the energy discharge tube, respectively. In a horizontal triple-tube LHTES unit numerical simulations showed, that for longitudinal fins keeping constant the fins volume, increasing the fins length and decreasing their thickness reduces the solidification time [23]. Longer thin fins penetrate deeper into the PCM medium which improves the discharge process. In a similar geometry Sarani et al. [24] showed that discontinuous fins can improve solidification and decrease the energy discharge time. Comparatively to longitudinal continuous fins, applying discontinuous fins can reduce up to 89% the discharge time. Liu et al. [25] studied numerically the energy discharge process of a high melting temperature salt. The results show that longitudinal fins with transversal triangular ramifications enhance the solidification rate [25]. This work also showed that increasing fins height accelerates the discharge process. Sciacovelli et al. [26] optimised the design of longitudinal Y-shaped combining CFD simulation with the response surface method. For the optimised fin design the results indicated an increase of 24% of the

system efficiency during the energy discharge. Lohrasbi et al. [27] studied the charge and discharge of a LHTES device with radial fins, regular longitudinal fins, and longitudinal V-shaped fins. The results indicated that all fins significantly enhance the discharge rate, V-shaped fins provided the lower discharge time, however the discharge rate was similar for the three fins arrangement studied. Regarding fins and nanoparticles application, numerical studies showed that combining fins and nanoparticles enhance the solidification rate [23,24]. However, simulations of the discharge process in a horizontal triple-tube LHTES with CuO nanoparticles and longitudinal fins, showed that for the same volume of extra material added (fins, nanoparticles and fins combined with nanoparticles), better results were obtained by applying fins only than fins combined with nanoparticles or using only nanoparticles alone [24]. Similar conclusions were reported for the solidification of PCM RT82 with Al₂O₃ nanoparticles and copper longitudinal fins [23]. For simultaneous charge and discharge conditions a faster thermal response was also reported due to the application of fins instead of Al₂O₃ nanoparticles [28].

Despite the extended literature already available regarding the effect of nano-additives and fins in the performance of thermal energy storage system based on PCMs. Most of the numerical studies were developed for coaxial 2D geometries and the thermal properties of the nano-enhanced PCMs employed to perform the simulations are generally obtained based on models. Furthermore, simulations often disregard HTF flow, employing mostly constant boundary conditions that the HTF wall interface, which limits the assessment of the effective energy discharge performance, making it impossible to analyse output temperatures and discharged heat. More so as the HTF simulated here has temperature-dependant properties (i.e. density, specific heat, viscosity and thermal conductivity) something uncommon in the literature, with the present study we aim to contribute to fill in this gap. In this work samples of commercial paraffin wax A53 doped with graphene-based nano-platelets were produced and characterised. Different types of nano-platelets, with diameters in the 1–15 µm range and thicknesses in the 6–15 nm range, were experimentally tested. The nanoparticles load varying from 0.5%wt up to 6%wt. Furthermore, full 3D numerical simulations were developed to analyse the impact of the nanoparticles and the fin pitch over the energy discharge process of a LHTES system equipped with a compact multi-pass finned tube HE. This geometry closely mimics the geometric features of the HE used ubiquitously in the HVAC industry, providing a solid base from which to develop this solution into a practical storage system application employing PCMs. The system performance was evaluated using the outlet temperature to make a comparison between delivered heat and useful delivered heat.

2. NePCM samples and experimental measurements

2.1. NePCM samples

The base PCM used in this work is an organic paraffin wax with the commercial designation of A53 (nominal melting temperature of 53 °C) provided by PCM Products Company. The graphite nano-platelets xGnP were provided by XG Sciences Inc. The graphite nano-platelets are ultrathin graphite particles that can also be thought of as short stacks of graphene sheets made with thickness ranging from a few nanometers and diameters ranging a few microns. Three different types of nano-platelets were employed: Grade M with thickness of 6–8 nm, diameter of 5 µm (M5) and of 15 µm (M15) and typical surface area of 120 to 150 m²/g; grade H with 15 µm thickness and 5 µm diameter (H5) and typical surface area of 50 to 80 m²/g and grade C that typically consist of aggregates of sub-micron platelets having diameter of less than two microns, typical thickness of a few nanometers and with a specific surface area of 750 m²/g (C750). These particles were chosen because of their superior thermal conductivity, comparable to that of carbon nanotubes, at a much less cost and thus feasible for applications.

Table 1
Graphene nanoplatelets properties.

Type	Diameter[nm]	Thickness[nm]	Specific surface - area [m ² /g]
M15	15	6–8	120–150
M5	5	6–8	120–150
C750	5	15	750
H5	<2000	^a	50–80

^aFew nm.

They also come with high dimensional aspect ratios that can be tailored to different sizes. The main geometric properties of the graphene nanoplatelets are presented in Table 1. To manufacture the NePCM samples the base PCM A53 was melted at 70 °C and the nano-platelets were added to the liquid paraffin at 0.5, 1, 2, 3, 4 and 6%wt, the liquid composite was magnetically stirred for 30 min.

2.2. Thermal properties measurements

The thermal properties of the pure and enhanced PCM samples were evaluated by laboratorial measurements. The thermal conductivity was measured by a modified enthalpy-based water bath method [29]. The specific heat capacity and fusion latent heat were measured by the Modulated Differential Scanning Calorimetry (MDSC) method. MDSC differs from the standard DSC in that it uses two simultaneous heating rates, a linear one that provides information similar to standard DSC, and a sinusoidal or modulated heating rate that permits the measurement of the sample's heat capacity.

2.3. Experimental data

The measured thermal conductivities, of the pure PCM and the NePCM samples for the different particles type are depicted in Fig. 1. The results show an overall increase in the thermal conductivity due to nano-platelets addition, the effect is not linear and differs for each particular type of nanoparticle's. The largest increase occurs for M15 samples, in the low regime up to 1%wt and for the fraction of 6%wt. The thermal conductivity enhancement does not present a monotonic evolution with the particle load. This behaviour was also reported by Fan and Khodadadi [7] for an organic PCM (cyclohexane) enhanced by copper oxide nanoparticles. For 1%wt M15 particles fraction (0.4%vol) the thermal conductivity was increased by 100% from the 0.22 W/m K for pure paraffin to the value of 0.44 W/m K and is multiplied by a factor of 3.5 for 6%wt (2.5%vol) particles load. The increase observed is similar to that found in the literature for a similar sized graphite nano-platelet of 15 µm diameter [15,16].

Nano-platelets M5 and M15 differ only in the diameter, H5 has the same diameter as M5 but smaller overall surface area. The samples added with M5 nano-platelets also exhibit a significant increase in the thermal conductivity, of the order of 60% to 100% for mass fractions between 2 and 6%wt (0.8%vol and 2.5%vol), the maximum value was obtained for 4%wt particles load. The composite with C750, the nano-platelets with the smaller size, more spherical shape and the larger surface area has less effect on the thermal conductivity than the rest, a small increase of 14%, rather constant for the whole range studied. At the higher end studied, 6%wt mass fraction for samples added with M5 and H5 nano-platelets, the enhancement is levelled or reduced in contrast to M15 in which the thermal conductivity is greatly enhanced.

The effects of the nanoparticles addition to A53 on the fusion latent heat value is presented in Fig. 2. It can be seen that for the mass fraction of 1%, in the case of samples M15, the thermal conductivity increases 100% and the fusion latent heat reduced by (2%). The fusion latent heat is gradually reduced with the increase of M15 fraction, for the mass fraction value of 6% the latent heat is reduced approximately 12% comparatively to the pure PCM. Similar trend was obtained for the samples with C750 nano-platelets. The values measured for the

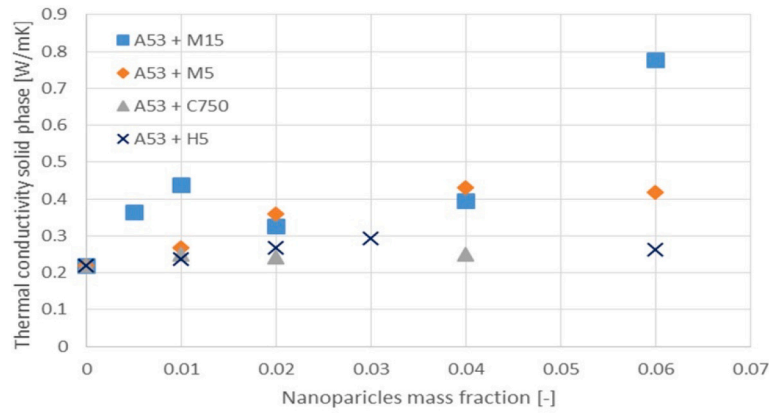


Fig. 1. Thermal conductivity of pure A53 and A53 NePCMs vs. nanoparticles mass fraction.

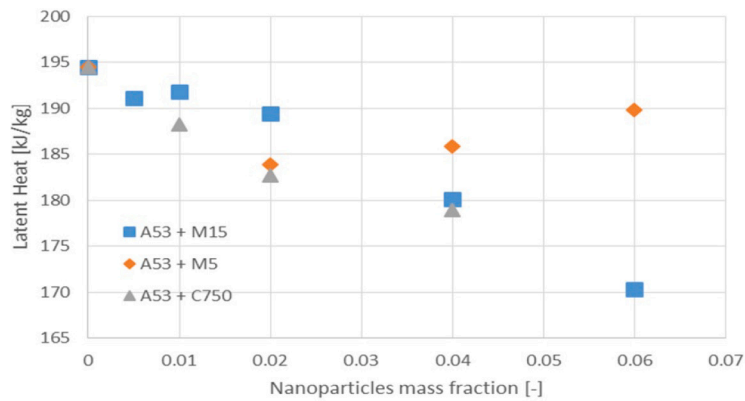


Fig. 2. Fusion latent heat of pure A53 and A53 NePCMs vs. nanoparticles mass fraction.

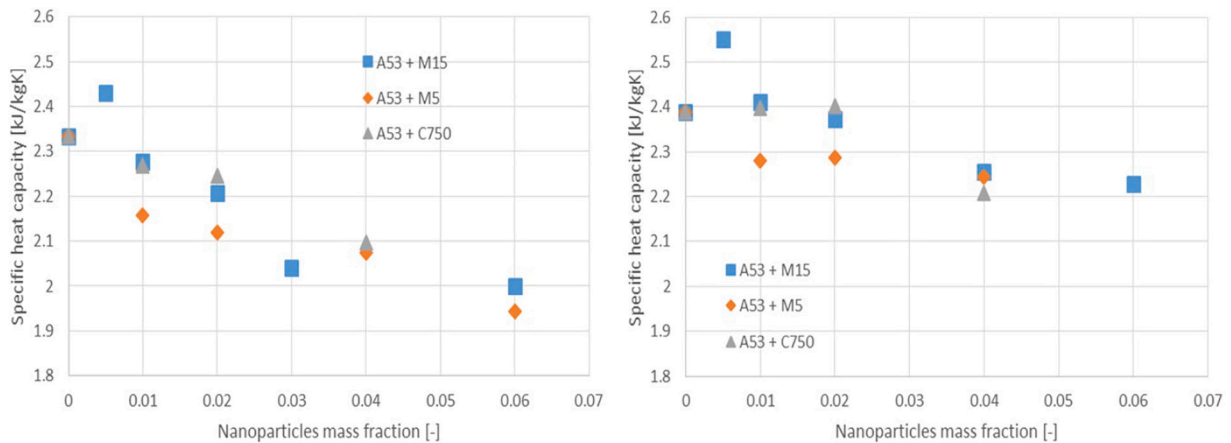


Fig. 3. Specific heat capacity of pure A53 and A53 NePCMs vs. nanoparticles mass fraction.

NePCM added with M5 nano-platelets presented a different evolution, this nano-platelets have a smaller effect on the latent heat at the larger mass fraction values.

The effect of the nanoparticle in the specific heat capacity for the solid and liquid phase is presented in Fig. 3. The maximum variation is less than 17% and occurs in the solid phase for M5 type particles at the 6%wt load. In the solid phase for M15 at 1%wt the reduction of the heat capacity comparatively to the pure PCM is 2% and at the higher mass fraction tested is 14%. In the liquid phase the effect of the nanoparticles in the specific heat capacity of the samples is smaller and follows the same trend than the solid phase for all particles type.

3. Numerical simulation

3.1. Mathematical model

The PCM solidification was simulated by the enthalpy-porosity formulation, the ability of this approach to model the solidification process of PCMs has been demonstrated in the past [23,24,30]. The complete numerical model solves the mass, momentum and energy transport equations for constant density. The viscous dissipation term is considered negligible while the energy equation is solved in the form of total

enthalpy.

$$\frac{\partial \rho}{\partial t} + \nabla \cdot (\rho \vec{v}) = 0 \quad (1)$$

$$\frac{\partial}{\partial t}(\rho \vec{V}) + \nabla \cdot (\rho \vec{V} \vec{V}) = -\nabla p + \mu \nabla^2 \vec{V} + \rho_o \beta (T - T_o) \vec{g} + \vec{S} \quad (2)$$

$$\frac{\partial \rho H}{\partial t} + \nabla \cdot (\rho \vec{V} H) = \nabla \cdot (k \nabla T) \quad (3)$$

\vec{V} represents the velocity, ρ the density, μ the dynamic viscosity, k the thermal conductivity, T the temperature and H the total enthalpy, defined as:

$$H = h + \Delta H \quad (4)$$

$$h = h_{ref} + \int_{T_{ref}}^T C_p dT \quad (5)$$

h represents the sensible enthalpy, C_p the specific heat and ΔH the phase change enthalpy. The temperature is calculated through the total enthalpy and the liquid mass fraction γ defined as:

$$\gamma = \begin{cases} 0 & , T < T_{solidus} \\ \frac{T - T_{solidus}}{T_{liquidus} - T_{solidus}} & , T_{solidus} < T < T_{liquidus} \\ 1 & , T > T_{liquidus} \end{cases} \quad (6)$$

Locally, the phase change enthalpy can be written in terms of the liquid mass fraction and the PCM latent heat, L , as, $\Delta H = \gamma L$. The enthalpy-porosity formulation treats different phases as a porous media by means of the following source term \vec{S} :

$$\vec{S} = \frac{(1 - \gamma)^2}{(\gamma^3 + \xi)} A_{mushy} \vec{v} \quad (7)$$

A_{mushy} is the mushy zone constant which describes how steeply the velocity is reduced to zero when the material solidifies. This is usually a very large value, ranging between 10^4 and 10^8 kg/(m³s), in the present study a standard value of $A_{mushy} = 10^5$ is employed. The constant ξ is a small value, in this case 10^{-3} , introduced to prevent division by zero.

The effect of natural convection in the PCM was accounted for by the Boussinesq approximation. This approach considers the density of fluid as a constant value in the governing equations, except for the source terms of the momentum equation that models buoyancy, in which the density temperature dependence is modelled according to the following equation:

$$\rho = \rho_o(1 - \beta(T - T_o)) \quad (8)$$

where ρ_o represents the PCM liquid density, β is the thermal expansion coefficient and T_o is defined as $T_o = (T_s + T_l)/2$ the subscript s and l indicate solidus and liquidus respectively. The HTF flow turbulence was simulated by the standard k-epsilon model [31] and buoyancy effects were neglected. In internal flows of liquid with small density variation the velocity field is dominated by pressure and friction effects.

3.2. Computational details and cases

The simulated geometry is a rectangular tank with a compact finned tube heat exchanger with copper tubes and aluminium fins. This HE type was selected because it is commonly used in commercial applications and can be manufactured with a great variety of tubes and fins patterns. Furthermore, compact finned tubes HEs have one the most suitable typologies for latent thermal energy storage applications because they combine a large storage capacity per unit volume with high heat transfer rates [32]. The ability of a PCM storage prototype equipped with multi-pass finned tubes HE, for meeting the requirements of domestic hot water applications, have been recently experimentally demonstrated [33]. The exterior dimensions of the tank are 500 mm in length, 146 mm in width and 195 mm in height, a sketch of one of the geometries simulated is presented in Fig. 4. The HE has a single circuit six meters long (not accounting for the bends). The circuit

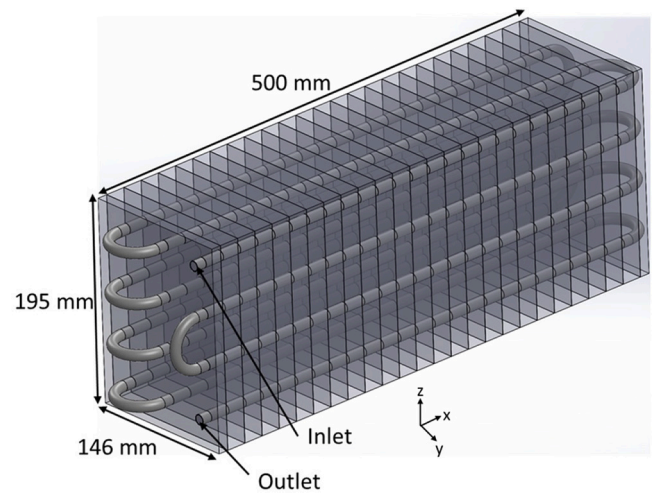


Fig. 4. LHTES simulated geometry.

has 12 passages in a parallel arrangement, the distance between the tubes centre is 49 mm. The tubes have an internal diameter of 8.6 mm and 10 mm of external diameter. The fins have 0.3 mm thickness and simulations were done for three fin pitch values, 20, 10 and 5 mm. Water was used as HTF, the inlet was through the top tube and the outlet from below.

The numerical simulations were performed for organic PCM A53 and A53 doped with M15 graphene nanoparticles at 1%wt and 6%wt fraction. The values of the latent heat, the specific heat and thermal conductivity of the pure PCM and NePCM considering in the simulations were the values experimentally measured and displayed in Figs. 1–3. It was assumed that the values do not change within the narrow range of the PCM operating temperature simulated. The thermal conductivity was considered to be equal for both phases. Table 2 summarises the materials' properties used in the numerical simulations for the pure A53, A53 enhanced by the nanoparticles and the HE materials, Copper and Aluminium. The increase of the dynamic viscosity of the PCM samples due to the nanoparticles were estimated based on the following correlation [34]:

$$\mu_{NePCM} = 0.983e^{(12.959\phi_n)} \mu_{PCM} \quad (9)$$

μ represents the dynamic viscosity, ϕ the nanoparticles volume fraction and the subscript n and PCM indicates nanoparticle and PCM. For HTF the specific heat, density, and viscosity were defined as a function of the temperature, for a range from 20 to 60 °C based on the data mentioned in [35].

The simulations were performed for fully turbulent conditions with a mass flow rate of 0.069 kg/s (4.18 l/min). The average velocity is 1.2 m/s, which is near the maximum recommended value for flows inside copper tubes in the range of temperature considered in the situations [36]. The Re_d number is ≈ 17700 , calculated based on the water inlet conditions. The turbulent regime was chosen because is the most common on practical systems. The initial temperature of the system was 54 °C and the water inlet temperature was 47.2 °C, five degrees below the PCM solidus temperature.

The simulated cases are summarised in Table 3, the latent energy storage capacity of each case was calculated based on the net volume around the tubes and fins, filled by PCM, and the density and fusion latent heat values of the pure and nanoparticles enhanced PCM samples. Table 3 also displays presents the ratio between the net volume around the HEs and the correspondent volume without fins.

Table 2
Material properties.

Property	Water	A53	A53 + 1%wt NP	A53 + 6%wt NP	Copper	Aluminium
ρ [kg/m ³]	Variation(20–60 °C)	775	780	806	8978	2719
Cp_s [J/kg K]	–	2270	2277	1999	381	871
Cp_l [J/kg K]	Variation(20–60 °C)	2400	2410	2228	–	–
k [W/m K]	Variation(20–60 °C)	0.22	0.44	0.78	378.6	202.4
μ [kg/m s]	Variation(20–60 °C)	0.0059	0.0060	0.0077	–	–
β [1/K]	Variation(20–0 °C)	0.0001	0.0001	0.0001	–	–
Melting latent heat [kJ/kg]	–	195	192	170	–	–
Solidus temperature [°C]	–	52.2	52.2	52.2	–	–
Liquidus temperature [°C]	–	53.6	53.6	53.6	–	–

s-Solid phase; l - Liquid phase.

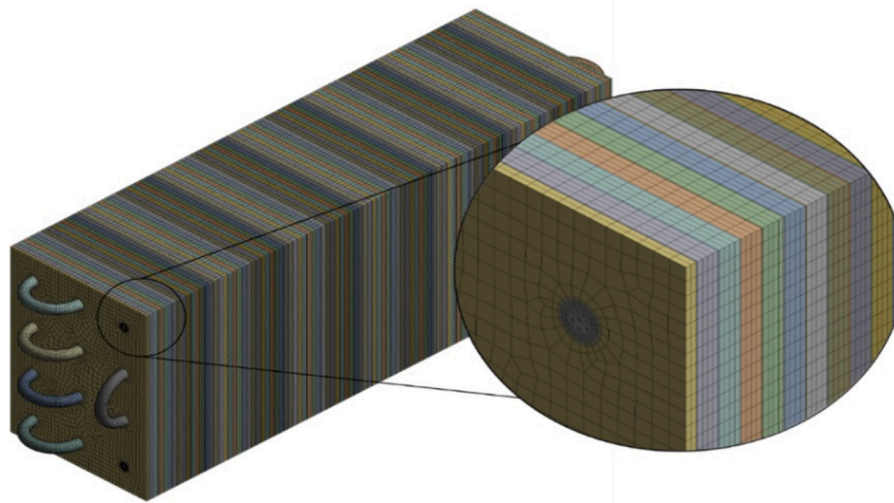


Fig. 5. Mesh and computational domain of the 5 mm fin pitch geometry.

Table 3
Simulated cases.

Case	Number of fins	Fin pitch [mm]	PCM/NePCM	Volume ratio [–]	Latent energy storage capacity [kJ]
A1	25	20	A53	0.985	2049
A2	25	20	A53 + 1%wt NP	0.985	2030
A3	25	20	A53 + 6%wt NP	0.985	1858
B1	50	10	A53	0.970	2018
B2	50	10	A53 + 1%wt NP	0.970	1999
B3	50	10	A53 + 6%wt NP	0.970	1829
C1	100	5	A53	0.940	1955
C2	100	5	A53 + 1%wt NP	0.940	1938
C3	100	5	A53 + 6%wt NP	0.940	1773

3.2.1. Computational details

The simulations were run with Fluent 19 code. The SIMPLE algorithm was used to couple velocity and pressure fields. The equations of the turbulent quantities, energy and momentum were discretised by second order upwind scheme and for the pressure the PRESTO scheme was used. The tank exterior surfaces were modelled as adiabatic walls. The HTF inlet boundary was set as velocity inlet and the outlet boundary was modelled as outflow flow type boundary. The computational mesh for all cases has a superior density inside the HTF circuit, in particular near the tube wall, to capture any effect of turbulence boundary layer in the flow field and in the heat transfer rate on the interior wall that may occur. Fig. 5 shows the computational domain and the mesh of one of the HE geometries.

The convergence criteria for mass, velocity and turbulent quantities transport equations were 10^{-3} and 10^{-8} for the energy equation. These values ensure convergence and were selected based on trial runs. Simulations were also developed to ensure mesh and time step

independent results. The trial runs showed that reducing the time step size below 0.25 s has a marginal effect on the results. Concerning mesh independence Fig. 6 shows the PCM liquid fractions evolution over time for three different meshes, the difference between the results is small and it is clear that the 3.7×10^6 elements mesh provides mesh independent results. The numerical results presented below were obtained with a time step size of 0.25 s and using three different meshes. The simulations for 20 mm fin pitch geometry were developed with a 3.1×10^6 elements mesh, a mesh with 3.3×10^6 elements was employed to simulate the 10 mm fin pitch geometry and a 3.7×10^6 elements mesh was used for 5 mm fin pitch geometry. The employed meshes do not have exactly the same elements because of the slight differences of the HEs geometries.

The machine used to run the numeric work was an Intel Xeon W-2155 3.30 GHz processor with RAM 63 GB and graphic card GPU NVIDIA Quadro P4000. The time for each case to run varied mostly with regards to the respective geometry, specifically with the of number of fins, the run times were between 300 for the cases with higher fin count and closer to 600 h for the cases with fewer fins, with the nanoparticles concentration also influencing the time.

4. Results and discussion

An analysis of the results was conducted for the different techniques in use and how it influenced the discharge process for the chosen geometries. Figs. 7 and 8 illustrate the distribution of the temperatures and the liquid mass fraction of cases A1 and A3, at three different stages of the solidification process, with three different planes, two planes cross the LHTES system longitudinally between the tubes, and another transversal plane that crosses the middle section of the HE. Figs. 9 and 10 depicts the corresponding images for cases C1 and

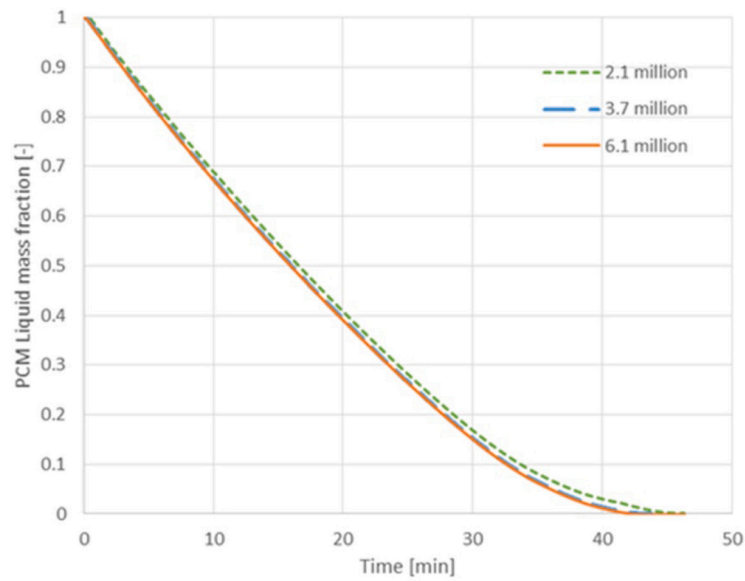


Fig. 6. Mesh independent study at 0.25 s time step (case C1).

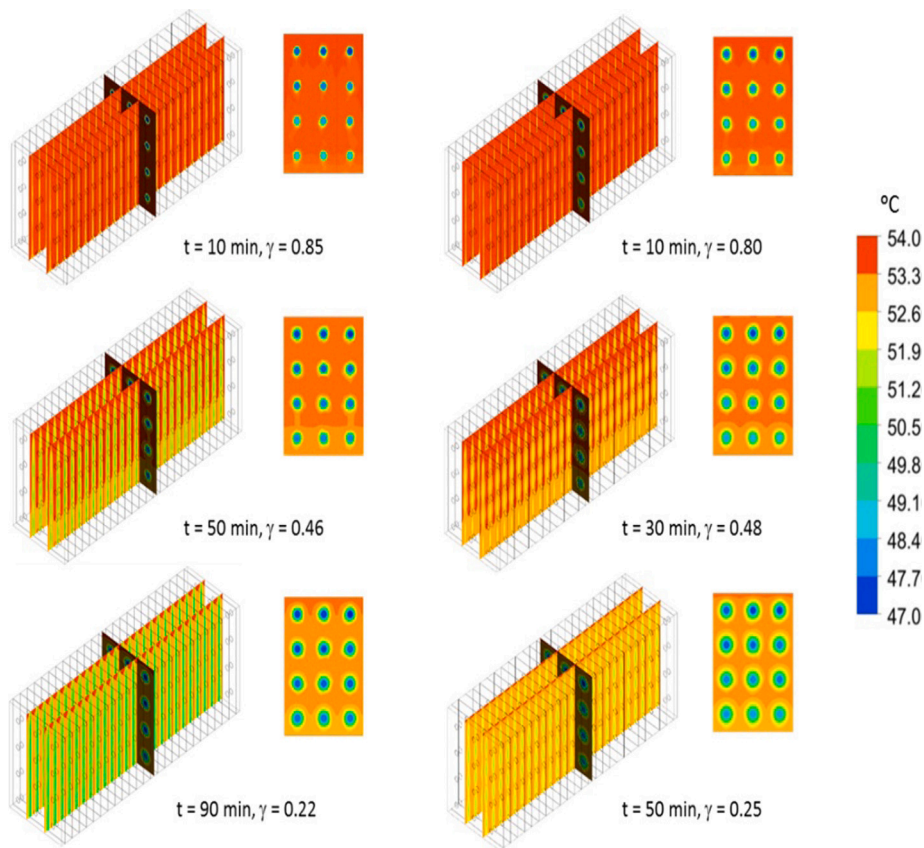


Fig. 7. Temperature distribution at three stages of the solidification process (left: case A1; right: case A3).

C3. The results showed that nanoparticles accelerate the solidification process. However, for each one of the three pitches the distribution of the temperatures and liquid mass fractions, in similar stages of the discharge process, are qualitatively similar for the pure PCM and the 6%wt GnP enhanced PCM. On the contrary, the effect on the fin pitch on solidification is clear. For 20 mm fin pitch (cases A1 and A3) the solidification process is characterised by temperature gradients and the liquid mass fraction between the fins. At each stage of the discharge process the contours of the transversal middle plan shows the

progress development of the solidification front uniform around all tube cross sections. As solidification advances, the gradient between the fins becomes more evident and it is possible to also observe temperature gradients and the liquid mass fraction across the vertical direction. The temperature increases from bottom to top, and the liquid mass fraction exhibits an inverse evolution. This suggests that convection streams transport the colder and denser PCM down and the hotter and lighter PCM up. The PCM between the fins, at the top of the tank, is the last material to solidify as shown in the last stages of Fig. 8. For the 5 mm

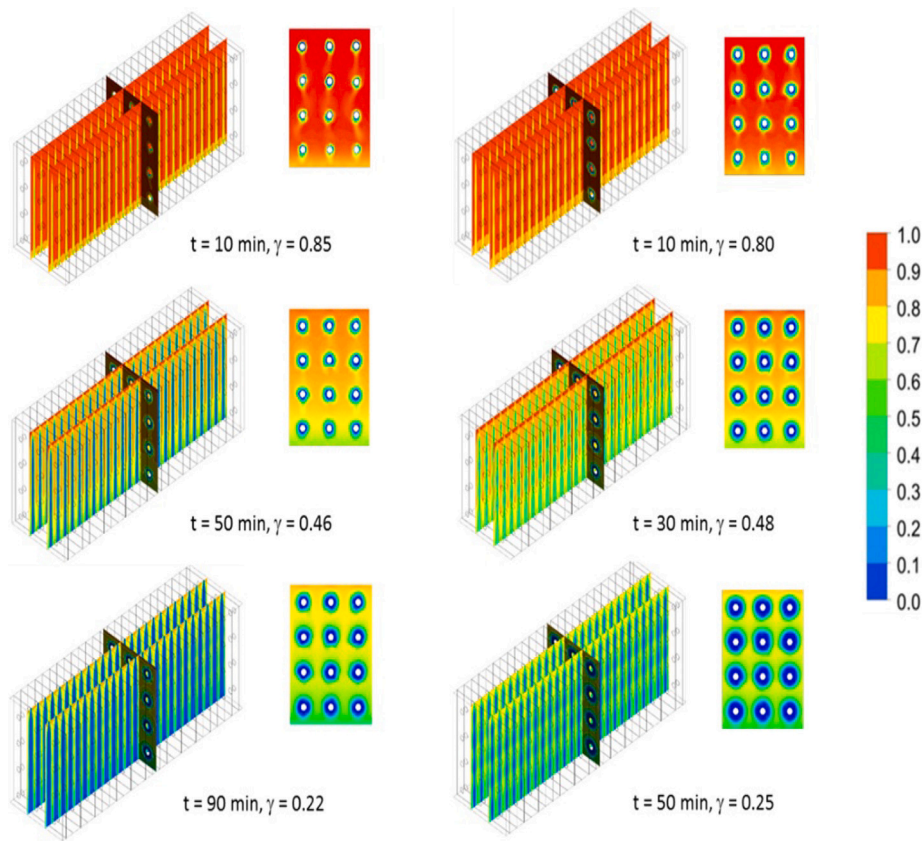


Fig. 8. Liquid mass fraction distribution at three stages of the solidification process (left: case A1; right: case A3).

fin pitch cases the solidification process is more homogeneous. The main temperature gradients are around the tube sections over great part of the discharge process. Only in the later stage of solidification the temperature shows gradients over the longitudinal planes, decreasing from top to bottom. The internal distribution of the liquid mass fraction displays a similar trend. The liquid mass fraction distribution on the middle transversal plane shows that, at each stage of the discharge process, the solidification front develops inversely to the HTF flow circulation. Solidification it is more developed around the tube cross sections near the HTF inlet and is progressively less developed as it approaches the outlet. This indicates that for the 5 mm fin pitch cases the discharge process is dominated by thermal diffusion.

The time progression of the solidification process and the HTF outlet temperature during solidification are displayed in Figs. 11 and 12. The solidification process is characterised by the continuous decrease of the HTF outlet temperature. The outlet temperature, of the cases with 10 and 20 mm fin pitch and with the nanoparticle enhanced paraffin, has a larger gradient at the beginning of the process comparatively to the other ones. Solidification starts forming a layer of solid material over the surfaces of the fins and around the tubes, for the NePCM cases, the layer of solid material grows quickly increasing the thermal resistance between the liquid PCM and HTF that decreases the heat transfer rate and consequently the HTF outlet temperature. For the other cases, this effect is lessened due to the PCM lower thermal conductivity and due to the larger total fin area. This smooths the HTF outlet temperature evolution at the early stages of the solidification process and explains the differences between the cases. The final stage of solidification is characterised by a sudden decrease of the outlet temperature for all cases. At full solidification the HTF outlet temperature comes close to the inlet value, which indicates that not all the discharged energy during the PCM solidification is useful energy.

The results clearly indicated that the fin pitch has a great impact in the solidification rate and nano-additives benefit becomes more

important as the fin pitch increases. The full solidification time is reduced almost 60%, from 188 min to approximate 77 min with the reduction of the fin pitch from 20 mm (case A1) to 10 mm (Case B1). For the 5 mm fin pitch case (C1) the time to achieve full solidification is less than 45 min which represents a reduction of 77% comparatively to case A1 and 43% to case B1. The discharge rate is also accelerated by the GnP, it is clear that the benefit of nano-additives increases with the fin pitch. For the fin pitch of 20 mm adding 1%wt GnP (case A2) reduces the full discharge time approximately 37% to 122 min. For 6%wt nanoparticles load (case A3) the reduction is higher, the time to achieve full solidification is 92 min which represents a reduction in 51% comparatively to the base PCM (case A1) case and 25% for the 1%wt NP. For the 10 mm fin pitch the advantage of the nanoparticles enhancement is lower, comparatively to the pure A53 (case B1) the full solidification time is reduced approximately 18%, from 77 min to 63 min, due to 1%wt GnP additions (case B2) and 31% to 53 min for the 6%wt NP case (Case B3). Finally, for the 5 mm fin pitch heat exchanger the results showed that adding nanoparticles to the PCM has little effect on the full discharge time. Comparatively to the pure A53 case (case C1) the maximum reduction is 11%, from 45 min to 37.5 min, for the 6%wt particles load (case C3). Adding 1%wt (case C2) of nanoparticles decreases the discharge time less than 6.5% to 42.1 min.

The data shown in Fig. 11 also indicates that, concerning the discharge rate enhancement in multi passages finned tube heat exchangers, increasing the area of fins in contact with the PCM is more effective than enhancing the PCM thermal conductivity. As it can be see comparing the solidification curves of cases A1, A2 and B1. The PCM thermal conductivity of cases A1 and B1 are the same and the fin area of case B1 doubled the fin area of case A1. On the other hand, case A2 and case A1 have the same fin area and the NePCM thermal conductivity of case A2 doubles the pure A53 thermal conductivity of case A1. However, the solidification process is faster for case B1 than case A2. The same can be said based on the results of cases B1, B2 and C1,

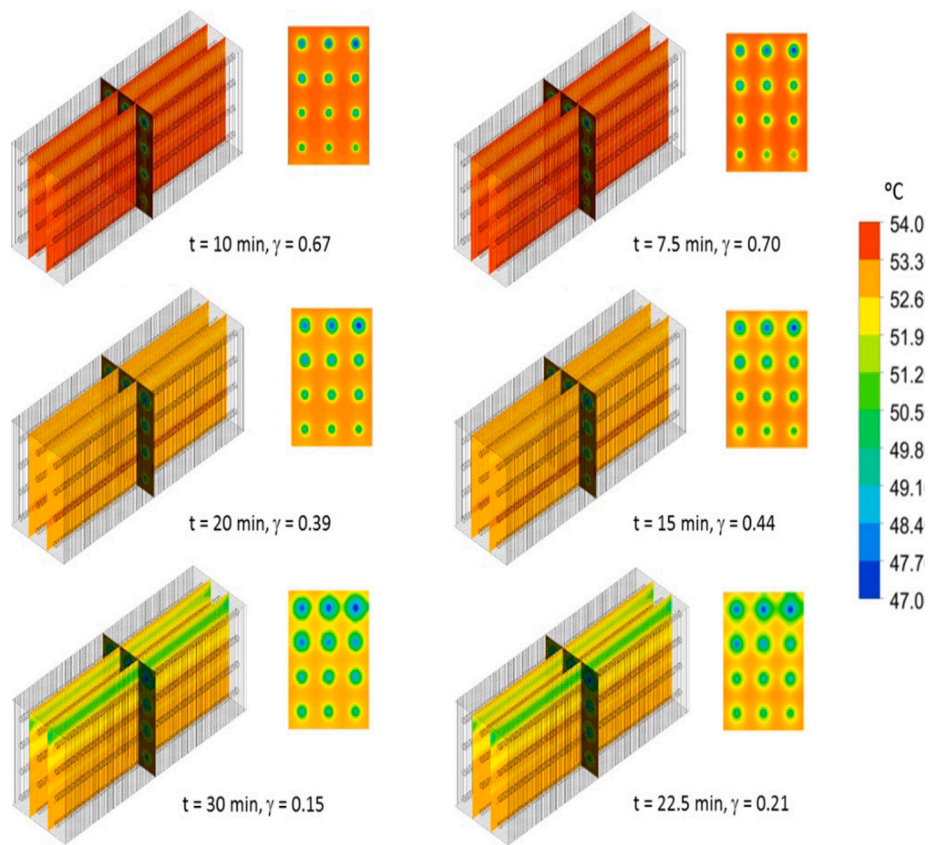


Fig. 9. Temperature distribution at three stages of the solidification process (left: case C1; right: case C3).

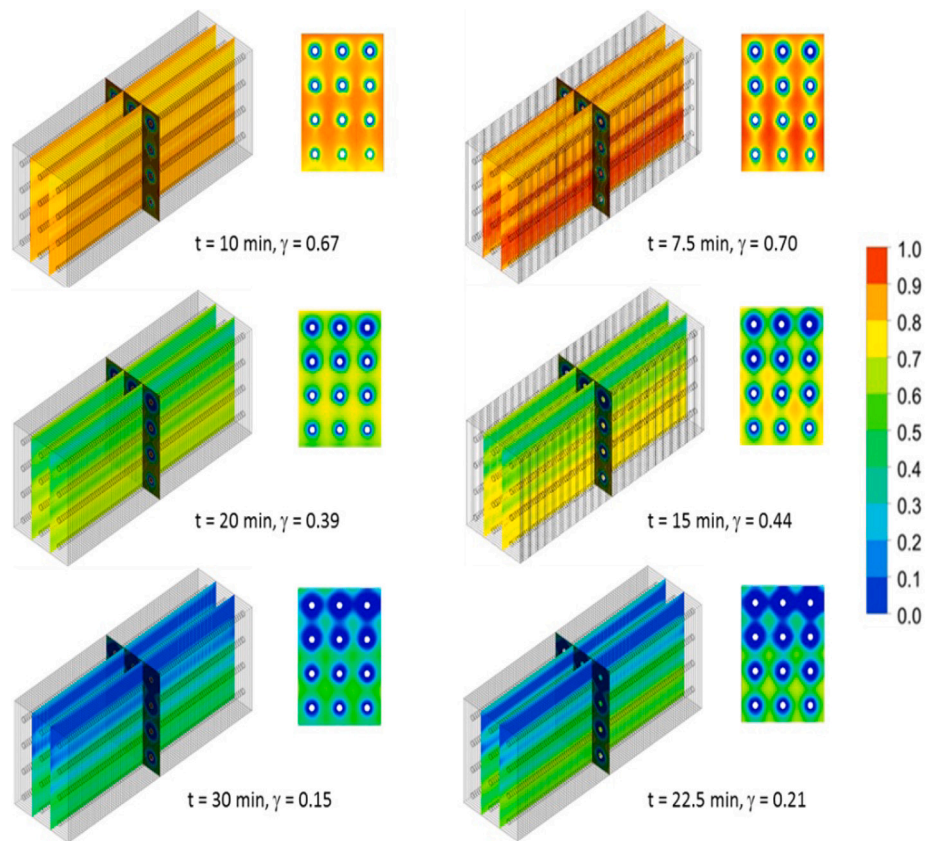


Fig. 10. Liquid mass fraction distribution at three stages of the solidification process (left: case C1; right: case C3).

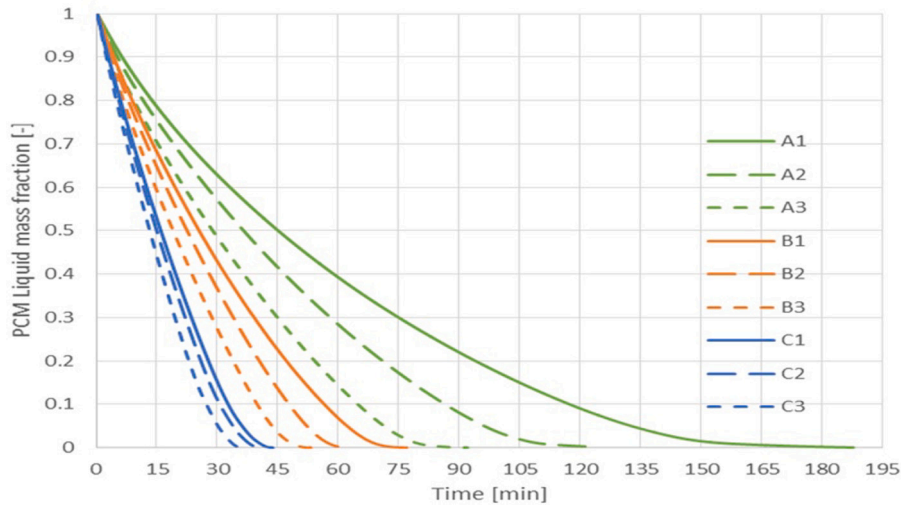


Fig. 11. Liquid fraction history.

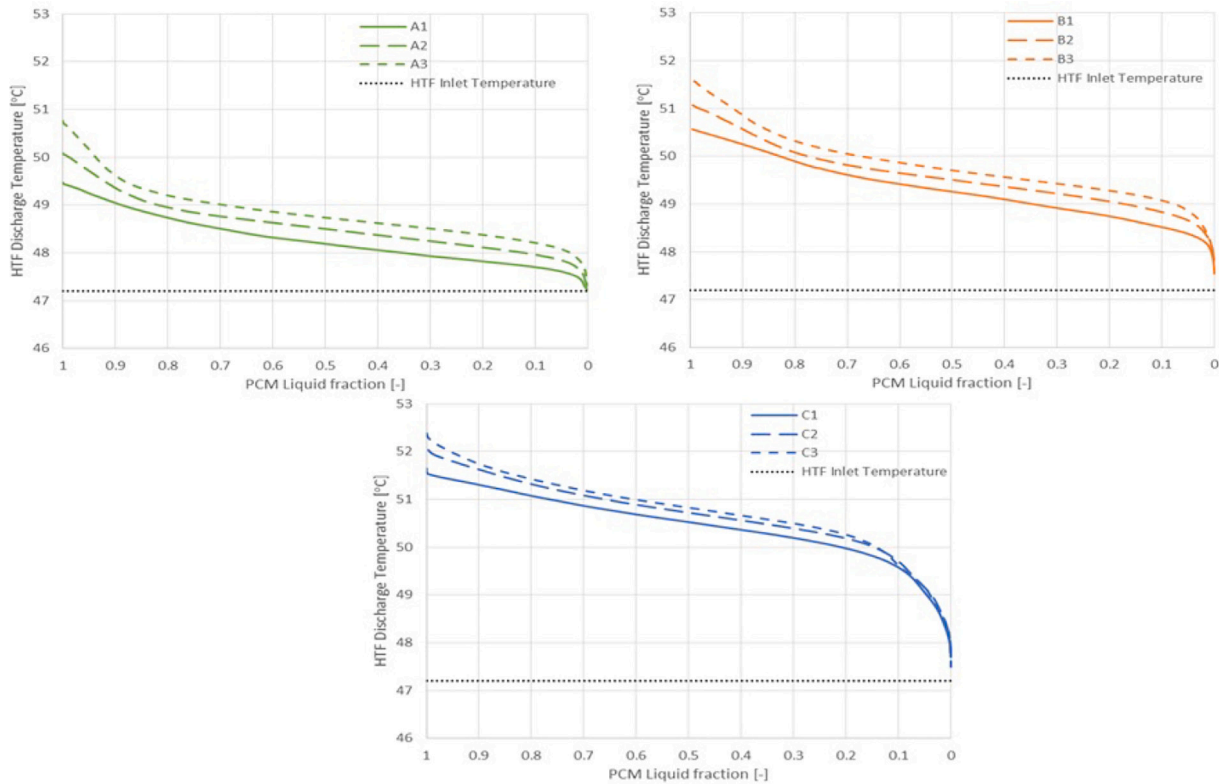


Fig. 12. HTF outlet temperature over solidification.

nevertheless the differences between the solidification curves of these cases are smaller. Furthermore, the results of cases A1, A3 and B1 and cases B1, B3 and C1 showed that doubling the fin area provides even better results than enhancing the PCM thermal conductivity medium by a factor of 3.5.

On one hand fin addition decreases the PCM inside storage system and consequently the system’s latent storage capacity, on the other hand, fins added mass to the system, which increases the capacity of stored sensible energy. Nanoparticles change the PCMs properties, which also affects the thermal energy storage capacity. To assess the effect of the fin pitch and the nanoparticles additions in the system energy discharge capacity Fig. 13 showcases the thermal energy discharged at

three stages of the solidification process. One stage at PCM full solidification and two for the instants until the HTF outlet temperature is higher than 49 °C and 50 °C. The discharged energy was calculated by the time integration of the heat transfer rate from the tubes wall to the HTF. Fig. 13 also shows the latent storage capacity for an equivalent, hypothetical system without fins and nanoparticles evaluated based on the properties of pure A53 and the system storage volume capacity without fins. Fig. 13 shows that, for all cases with a load of NP ≤1%wt, the thermal discharged energy at full solidification, combining latent and sensible heat, is superior to the latent heat storage capacity of the equivalent system without fins and nanoparticles. Case C3 presented the worst results in which the amount of thermal discharge energy at full solidification is 93% of the latent heat storage capacity of the

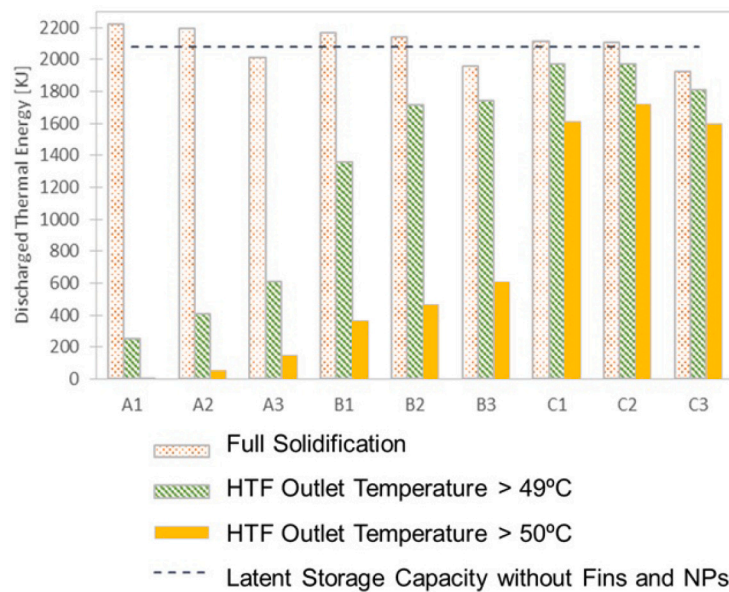


Fig. 13. Thermal energy discharge capacity at different stages of solidification.

equivalent system without fins and NP. Nevertheless, the system ability for delivering useful heat is better assessed based on the discharged thermal energy for the HTF outlet temperature >49 °C and >50 °C. The data presented in Fig. 13 clearly shows the benefits of add fins, the capacity for discharge heat at both temperature levels, increases significantly with the reduction of the fin pitch. This is particularly important for the upper temperature scenario. The thermal energy discharged for the HTF temperature >50 °C, is marginal for case A1 and for case C1 is 1595 kJ, which represents 89.8% of latent storage capacity of this case (see Table 3).

Combining fins and nanoparticles can improve the thermal energy discharge performance. However, the effect of NP depends on the fin pitch and the required level of the HTF outlet temperature. For the 20 mm and 10 mm fin pitch, the capacity for delivering useful heat increases with the GnP load for both values of the HTF outlet temperature. Nevertheless, for the 20 mm fin pitch cases despite the nanoparticles the discharged energy is low for both temperature levels. Below 150 kJ for the 50 °C and just 610 kJ for the 49 °C, in both cases obtained combining the fins with 6%wt particles load. For the 10 mm fin pitch and for the HTF outlet temperature >49 °C, combining fins and 1%wt GnP increases the discharge energy capacity 22.3%, from 1357 kJ to 1714 kJ. Increasing the GnP load from 1%wt to 6%wt increases the heat discharge capacity less than 2% to 1740 kJ. For the HTF temperature >50 °C, even for the 6%wt GnP load the maximum capacity of discharge thermal energy is just 604 kJ (case B3), which represents only 33.1% of the latent storage capacity. Concerning the 5 mm fin pitch cases (C1, C2 and C3 cases) the useful heat discharge capacity presents different evolution according with the HTF outlet temperature requirements. For the HTF outlet temperature >49 °C, comparatively to employing fins alone, combining fins and NP at 1%wt load does not affect the thermal energy discharged and increasing the NP load to 6%wt has a negative impact on this value. Regarding the capacity for discharging heat above 50 °C, the results show that fins alone and combining fins with 6%wt NP provide similar results. The best result is obtained combining fins with 1%wt NP. Nevertheless, for both temperatures, the influence of the NP in the heat delivered capacity is relatively small. For the 49 °C, the discharge heat capacity of case C3 is reduced 8.2% comparatively to case C1 and for the 50 °C the increment of the discharged useful heat due to the GnP (case C2) comparatively to the use of fins alone is 6.4%.

5. Conclusions

This work analysed the heat discharge process of a latent energy storage system. Firstly, the enhancement of an organic PCM thermal conductivity through addition of graphene nano-platelets was investigated. Particles with different shapes and sizes at various concentrations were employed. The thermal conductivities specifically, the heat capacity and fusion latent heat of the pure and enhanced PCM samples were evaluated by experimental measurements. Resorting to the gathered experimental data, CFD simulations were developed to assess the effect of nano-additives and fin pitch on the discharge performance of a LHTES system with a multi pass finned tube HE under full turbulent conditions of the HTF flow.

The results showed that paraffin A53 thermal conductivity is significantly enhanced by the dispersion of graphene nano-platelets nanoparticles at low concentrations. The addition of only 1wt% GnP with high aspect ratio (M15 Type) doubles the PCMs' thermal conductivity and for 6wt% the thermal conductivity increases by a factor of 3.5, in turn, the fusion latent heat of the samples is reduced between 2% to 12%.

The CFD simulations showed that combining fins and nanoparticles improve the thermal energy discharge performance. However, the effect of NP depends on the fin pitch and the required level of the HTF discharge temperature. For both outlet temperatures, the influence of the NP in the heat delivered capacity is relatively small. Reducing the fin pitch, as a single modification, has a great impact on the discharge rate and significantly enhances the useful heat discharge capacity. The role of nanoparticles on the solidification rate and the effective thermal energy discharge capacity becomes secondary with the reduction of the fin pitch. In the range of the studied fin pitch, doubling the fin surface area in contact with the PCM provided a greater improvement of the system discharge performance than enhancing the thermal conductivity of the PCM medium by a factor of 3.5 via nanoparticles enhancement.

Ultimately, the results demonstrated that, for latent heat storage application systems, the disadvantages related with the poor thermal conductivity of common PCMs, can be surpassed without penalising the useful heat discharge capacity by employing a general purpose HVAC finned tubes HEs with the proper fin design and sizing.

Declaration of competing interest

The authors declare that they have no known competing financial interests or personal relationships that could have appeared to influence the work reported in this paper.

Acknowledgments

This work was partially financially supported by the TESSE2b project that has received funding from the European Union's Horizon 2020 research and innovation programme under grant agreement No 680555. This article reflects only the authors' view and the European Commission is not responsible for any use that may be made of the information it contains.

References

- [1] S. Kalnæs, B. Jelle, Phase change materials and products for building applications: A state-of-the-art review and future research opportunities, *Energy Build.* 94 (2015) 150–176, <http://dx.doi.org/10.1016/j.enbuild.2015.02.023>.
- [2] A. Sharma, V. Tyagi, C. Chen, D. Buddhi, Review on thermal energy storage with phase change materials and applications, *Renew. Sustain. Energy Rev.* 13 (2) (2009) 318–345, <http://dx.doi.org/10.1016/j.rser.2007.10.005>, URL <https://linkinghub.elsevier.com/retrieve/pii/S1364032107001402>.
- [3] A. Sari, A. Karaipekli, Thermal conductivity and latent heat thermal energy storage characteristics of paraffin/expanded graphite composite as phase change material, *Appl. Therm. Eng.* 27 (8–9) (2007) 1271–1277, <http://dx.doi.org/10.1016/j.applthermaleng.2006.11.004>, URL <https://linkinghub.elsevier.com/retrieve/pii/S1359431106004030>.
- [4] A. Fleming, S. Wena, L. Shi, A. da Silva, Experimental and theoretical analysis of an aluminium foam enhanced phase change thermal storage unit, *Int. J. Heat Mass Transfer* 82 (2015) 273–281, <http://dx.doi.org/10.1016/j.ijheatmasstransfer.2014.11.022>.
- [5] J. Fukai, Y. Hamada, Y. Morozumi, O. Miyatake, Effect of carbon-fiber brushes on conductive heat transfer in phase change materials, *Int. J. Heat Mass Transfer* 45 (24) (2002) 4781–4792, [http://dx.doi.org/10.1016/S0017-9310\(02\)00179-5](http://dx.doi.org/10.1016/S0017-9310(02)00179-5), URL <https://linkinghub.elsevier.com/retrieve/pii/S0017931002001795>.
- [6] J. Fukai, M. Kanou, Y. Kodama, O. Miyatake, Thermal conductivity enhancement of energy storage media using carbon fibers, *Energy Convers. Manage.* 41 (14) (2000) 1543–1556, [http://dx.doi.org/10.1016/S0196-8904\(99\)00166-1](http://dx.doi.org/10.1016/S0196-8904(99)00166-1), URL <https://linkinghub.elsevier.com/retrieve/pii/S0196890499001661>.
- [7] L. Fan, J. Khodadadi, An experimental investigation of enhanced thermal conductivity and expedited unidirectional freezing of cyclohexane-based nanoparticle suspensions utilized as nano-enhanced phase change materials (NEPCM), *Int. J. Therm. Sci.* 62 (2012) 120–126, <http://dx.doi.org/10.1016/j.ijthermalsci.2011.11.005>, URL <https://linkinghub.elsevier.com/retrieve/pii/S1290072911003358>.
- [8] S. Jesumathy, M. Udayakumar, S. Suresh, Experimental study of enhanced heat transfer by addition of CuO nanoparticle, *Heat Mass Transf.* 48 (6) (2012) 965–978, <http://dx.doi.org/10.1007/s00231-011-0945-y>, URL <http://link.springer.com/10.1007/s00231-011-0945-y>.
- [9] J.L. Zeng, L.X. Sun, F. Xu, Z.C. Tan, Z.H. Zhang, J. Zhang, T. Zhang, Study of a PCM based energy storage system containing Ag nanoparticles, *J. Therm. Anal. Calorim.* 87 (2) (2007) 371–375, <http://dx.doi.org/10.1007/s10973-006-7783-z>, URL <http://link.springer.com/10.1007/s10973-006-7783-z>.
- [10] T.-P. Teng, C.-C. Yu, Characteristics of phase-change materials containing oxide nano-additives for thermal storage, *Nanoscale Res. Lett.* 7 (1) (2012) 611, <http://dx.doi.org/10.1186/1556-276X-7-611>, URL <https://nanoscalereslett.springeropen.com/articles/10.1186/1556-276X-7-611>.
- [11] M. Khodadadi, M. Sheikholeslami, Heat transfer efficiency and electrical performance evaluation of photovoltaic unit under influence of NEPCM, *Int. J. Heat Mass Transfer* 183 (2022) 122232, <http://dx.doi.org/10.1016/j.ijheatmasstransfer.2021.122232>, URL <https://doi.org/10.1016/j.ijheatmasstransfer.2021.122232>.
- [12] R.J. Warzoha, A. Rao, R. Weigand, A.S. Fleischer, Experimental characterization of the thermal diffusivity of paraffin phase change material embedded with herringbone style graphite nanofibers, in: *Volume 2: Heat Transfer Enhancement for Practical Applications; Fire and Combustion; Multi-Phase Systems; Heat Transfer in Electronic Equipment; Low Temperature Heat Transfer; Computational Heat Transfer*, American Society of Mechanical Engineers, Rio Grande, Puerto Rico, USA, 2012, pp. 307–315, <http://dx.doi.org/10.1115/HT2012-58043>, URL <https://asmedigitalcollection.asme.org/HT/proceedings/HT2012/44786/307/245096>.
- [13] J.L. Zeng, Y.Y. Liu, Z.X. Cao, J. Zhang, Z.H. Zhang, L.X. Sun, F. Xu, Thermal conductivity enhancement of MWNTs on the PANI/tetradecanol form-stable PCM, *J. Therm. Anal. Calorim.* 91 (2) (2008) 443–446, <http://dx.doi.org/10.1007/s10973-007-8545-2>, URL <http://link.springer.com/10.1007/s10973-007-8545-2>.
- [14] M. Li, A nano-graphite/paraffin phase change material with high thermal conductivity, *Appl. Energy* 106 (2013) 25–30, <http://dx.doi.org/10.1016/j.apenergy.2013.01.031>, URL <https://linkinghub.elsevier.com/retrieve/pii/S0306261913000408>.
- [15] S. Kim, L.T. Drzal, High latent heat storage and high thermal conductive phase change materials using exfoliated graphite nanoplatelets, *Sol. Energy Mater. Sol. Cells* 93 (1) (2009) 136–142, <http://dx.doi.org/10.1016/j.solmat.2008.09.010>, URL <https://linkinghub.elsevier.com/retrieve/pii/S0927024808002857>.
- [16] J. Xiang, L.T. Drzal, Investigation of exfoliated graphite nanoplatelets (xGnP) in improving thermal conductivity of paraffin wax-based phase change material, *Sol. Energy Mater. Sol. Cells* 95 (7) (2011) 1811–1818, <http://dx.doi.org/10.1016/j.solmat.2011.01.048>, URL <https://linkinghub.elsevier.com/retrieve/pii/S0927024811000675>.
- [17] Z. Khan, Z. Ahmad Khan, Experimental and numerical investigations of nano-additives enhanced paraffin in a shell-and-tube heat exchanger: A comparative study, *Appl. Therm. Eng.* 143 (2018) 777–790, <http://dx.doi.org/10.1016/j.applthermaleng.2018.07.141>, URL <https://linkinghub.elsevier.com/retrieve/pii/S1359431118324190>.
- [18] N.S. Dhaidan, J. Khodadadi, T.A. Al-Hattab, S.M. Al-Mashat, Experimental and numerical study of constrained melting of n-octadecane with CuO nanoparticle dispersions in a horizontal cylindrical capsule subjected to a constant heat flux, *Int. J. Heat Mass Transfer* 67 (2013) 523–534, <http://dx.doi.org/10.1016/j.ijheatmasstransfer.2013.08.001>.
- [19] A.A.R. Darzi, M. Jourabian, M. Farhadi, Melting and solidification of PCM enhanced by radial conductive fins and nanoparticles in cylindrical annulus, *Energy Convers. Manage.* 118 (2016) 253–263, doi:Energy Conversion and Management.
- [20] W.-B. Ye, H.-J. Guo, S.-M. Huang, Y.-X. Hong, Research on melting and solidification processes for enhanced double tubes with constant wall temperature/wall heat flux, *Heat Transfer-Asian Res.* 47 (3) (2017) 583–599, <http://dx.doi.org/10.1002/htj.21328>.
- [21] S. Deng, C. Nie, G. Wei, W.-B. Ye, Improving the melting performance of a horizontal shell-tube latent-heat thermal energy storage unit using local enhanced finned tube, *Energy Build.* 183 (2019) 161–173, <http://dx.doi.org/10.1016/j.enbuild.2018.11.018>.
- [22] M. Rathod, J. Banerjee, Thermal performance enhancement of shell and tube Latent Heat Storage Unit using longitudinal fins, *Appl. Therm. Eng.* 75 (2015) 1084–1092, <http://dx.doi.org/10.1016/j.applthermaleng.2014.10.074>.
- [23] J.M. Mahdi, E.C. Nsofor, Solidification enhancement of PCM in a triplex-tube thermal energy storage system with nanoparticles and fins, *Appl. Energy* 211 (2018) 975–986, <http://dx.doi.org/10.1016/j.apenergy.2017.11.082>, URL <https://linkinghub.elsevier.com/retrieve/pii/S0306261917316811>.
- [24] I. Sarani, S. Payan, S. Nada, A. Payan, Numerical investigation of an innovative discontinuous distribution of fins for solidification rate enhancement in PCM with and without nanoparticles, *Appl. Therm. Eng.* 176 (2020) 115017, <http://dx.doi.org/10.1016/j.applthermaleng.2020.115017>, URL <https://linkinghub.elsevier.com/retrieve/pii/S1359431119358107>.
- [25] S. Liu, H. Peng, Z. Hu, X. Ling, J. Huang, Solidification performance of a latent heat storage unit with innovative longitudinal triangular fins, *Int. J. Heat Mass Transfer* 138 (2019) 667–676, <http://dx.doi.org/10.1016/j.ijheatmasstransfer.2019.04.121>, URL <https://linkinghub.elsevier.com/retrieve/pii/S0017931019307860>.
- [26] A. Sciacovelli, F. Gagliardi, V. Verda, Maximization of performance of a PCM latent heat storage system with innovative fins, *Appl. Energy* 137 (2015) 707–715, <http://dx.doi.org/10.1016/j.apenergy.2014.07.015>.
- [27] S. Lohrasbi, M. Gorji-Bandpy, D.D. Ganji, Thermal penetration depth enhancement in latent heat thermal energy storage system in the presence of heat pipe based on both charging and discharging processes, *Energy Convers. Manage.* 148 (2017) 646–667, <http://dx.doi.org/10.1016/j.enconman.2017.06.034>, URL <https://linkinghub.elsevier.com/retrieve/pii/S0196890417305800>.
- [28] J.M. Mahdi, S. Lohrasbi, D.D. Ganji, E.C. Nsofor, Simultaneous energy storage and recovery in the triplex-tube heat exchanger with PCM, copper fins and Al2O3 nanoparticles, *Energy Convers. Manage.* 180 (2019) 949–961, <http://dx.doi.org/10.1016/j.enconman.2018.11.038>, URL <https://linkinghub.elsevier.com/retrieve/pii/S0196890418312895>.
- [29] G.A. Evangelakis, I.E. Lagaris, D.G. Papageorgiou, K. Prouskas, A.E. Zisopoulou, A hybrid numerical-experimental method for determining thermal conductivities, *J. Heat Transfer* 143 (1) (2021) 011702, <http://dx.doi.org/10.1115/1.4048468>, URL <https://asmedigitalcollection.asme.org/heattransfer/article/doi/10.1115/1.4048468/1087174/A-Hybrid-Numerical-Experimental-Method-for>.
- [30] M. Longeon, A. Soupart, J.-F. Fourmigué, A. Bruch, P. Marty, Experimental and numerical study of annular PCM storage in the presence of natural convection, *Appl. Energy* 112 (2013) 175–184, <http://dx.doi.org/10.1016/j.apenergy.2013.06.007>.
- [31] W. Jones, B. Launder, The prediction of laminarization with a two-equation model of turbulence, *Int. J. Heat Mass Transfer* 15 (2) (1972) 301–314, [http://dx.doi.org/10.1016/0017-9310\(72\)90076-2](http://dx.doi.org/10.1016/0017-9310(72)90076-2), URL <https://linkinghub.elsevier.com/retrieve/pii/0017931072900762>.
- [32] M. Medrano, M. Yilmaz, M. Nogués, I. Martorell, J. Roca, L.F. Cabeza, Experimental evaluation of commercial heat exchangers for use as PCM thermal storage systems, *Appl. Energy* 86 (10) (2009) 2047–2055, <http://dx.doi.org/10.1016/j.apenergy.2009.01.014>, URL <https://linkinghub.elsevier.com/retrieve/pii/S030626190900021X>.
- [33] G. Dogkas, J. Konstantaras, M.K. Koukou, M. Gr. Vrachopoulos, C. Pagkalos, V.N. Stathopoulos, P.K. Pandis, K. Lympers, L. Coelho, A. Rebola, Development and experimental testing of a compact thermal energy storage tank using paraffin targeting domestic hot water production needs, *Therm. Sci. Eng. Prog.* 19 (2020) 100573, <http://dx.doi.org/10.1016/j.tsep.2020.100573>, URL <https://linkinghub.elsevier.com/retrieve/pii/S2451904920300913>.

- [34] J.M. Mahdi, S. Lohrasbi, D.D. Ganji, E.C. Nsofor, Accelerated melting of PCM in energy storage systems via novel configuration of fins in the triplex-tube heat exchanger, *Int. J. Heat Mass Transfer* 124 (2018) 663–676, <http://dx.doi.org/10.1016/j.ijheatmasstransfer.2018.03.095>, URL <https://linkinghub.elsevier.com/retrieve/pii/S0017931017333355>.
- [35] Water properties table. URL <https://www.pipeflowcalculations.com/tables/water.xhtml>.
- [36] Copper Tube Handbook, URL https://www.copper.org/publications/pub_list/pdf/copper_tube_handbook.pdf.